Intrinsic directionality of migrating vascular smooth muscle cells is regulated by NAD$^+$ biosynthesis

Hao Yin[1,*], Eric van der Veer[1,2,*], Matthew J. Frontini[1,2,*], Victoria Thibert[1,2], Caroline O'Neil[1], Alanna Watson[1,2], Peter Szasz[1], Michael W. A. Chu[3,4] and J. Geoffrey Pickering[1,2,4,‡]

[1]Robarts Research Institute, London, ON, Canada
[2]Departments of Medicine (Cardiology), Biochemistry and Medical Biophysics, University of Western Ontario, London, ON, Canada
[3]Department of Surgery, University of Western Ontario, London, ON, Canada
[4]London Health Sciences Centre, London, ON, Canada

*These authors contributed equally to this work
‡Author for correspondence (gpickering@robarts.ca)

Accepted 19 August 2012
Journal of Cell Science 125, 5770–5780

doi: 10.1242/jcs.110262

Summary

Cell migration is central to tissue repair and regeneration but must proceed with precise directionality to be productive. Directional migration requires external cues but also depends on the extent to which cells can inherently maintain their direction of crawling. We report that the NAD$^+$ biosynthetic enzyme, nicotinamide phosphoribosyltransferase (Nampt/PBEF/visfatin), mediates directionally persistent migration of vascular smooth muscle cells (SMCs). Time-lapse microscopy of human SMCs subjected to Nampt inhibition revealed chaotic motility whereas SMCs transduced with the Nampt gene displayed highly linear migration paths. Ordered motility conferred by Nampt was associated with downsizing of the lamellipodium, reduced lamellipodium wandering around the cell perimeter, and increased lamellipodial protrusion rates. These protrusive and polarity-stabilizing effects also enabled spreading SMCs to undergo bipolar elongation to an extent not typically observed *in vitro*. Nampt was found to localize to lamellipodia and fluorescence recovery of Nampt–eGFP after photobleaching revealed microtubule-dependent transport of Nampt to the leading edge. In addition, Nampt was found to associate with, and activate, Cdc42, and Nampt-driven directional persistence and lamellipodium anchoring required Cdc42. We conclude that high-fidelity SMC motility is coordinated by a Nampt–Cdc42 axis that yields protrusive but small and anchored lamellipodia. This novel, NAD$^+$-synthesis-dependent control over motility may be crucial for efficient repair and regeneration of the vasculature, and possibly other tissues.

Key words: Cell migration, Lamellipodia, NAD$^+$

Introduction

Adult vascular smooth muscle cells (SMCs) normally exist as stationary, contractile cells but they also have the capacity to migrate. The migratory SMC phenotype is crucial for vascular health because it enables SMCs to crawl to injured sites in the artery wall and participate in vessel repair. Efficient migration of SMCs is also central to preventing the often-fatal consequences of atherosclerosis, by stabilizing vulnerable and rupture-prone lesions (Dickson and Gotlieb, 2003; Falk et al., 1995; Naghavi et al., 2003).

A key determinant of effective cell migration is the extent to which the cell crawls in a direct path to its target site. Signal gradients in the local environment are important in this regard, with gradients of PDGF-BB being particularly so for vascular SMCs (Ferns et al., 1991; Pickering et al., 1997). However, it has recently been recognized that, in addition to external cues, there are intrinsic cellular attributes that determine whether a cell maintains a direct path of translocation or follows a more meandering route (Petrie et al., 2009). The relative contribution of intrinsic versus extrinsic control over directed cell migration varies among different cell types but may be particularly important for constitutively adherent cells (Pankov et al., 2005). Known mediators of intrinsically controlled directional persistence include Rho family GTPases, integrin signals and microtubules but it is clear that the regulation networks are complex and incompletely understood (Moissoglu and Schwartz, 2006; Pankov et al., 2005; Petrie et al., 2009).

Elucidating the innate pathways that promote directionally persistent migration can be limited by the fact that, in the absence of an applied chemoattractant gradient, cultured cells often display a random pattern of migration. This is the case for vascular SMCs, which are relatively slow moving cells that reorient and change direction frequently (Li et al., 2000; Rocnik et al., 1998). However, we have identified lines of human vascular SMCs that can be stimulated to migrate in a strikingly non-random pattern by withdrawing serum from the cultures (van der Veer et al., 2005). This straightforward manipulation promotes a switch from random migration to streaming of cells into aggregates. One protein found to be upregulated during this switch was nicotinamide phosphoribosyltransferase (Nampt), an NAD$^+$ biosynthetic enzyme that has also been known as pre B-cell colony enhancing factor and visfatin (van der Veer et al., 2007; van der Veer et al., 2005).

Nampt catalyzes the rate-limiting step in the synthesis of NAD$^+$ from nicotinamide. This particular biosynthetic pathway generates NAD$^+$ from dietary nicotinamide but also from

nicotinamide liberated intracellularly by enzymes that use NAD^+ as a substrate or co-substrate (Bogan and Brenner, 2008; Borradaile and Pickering, 2009). NAD^+-consuming enzymes include sirtuins, ADP-ribosyltransferases (ARTs) and NADases (Koch-Nolte et al., 2011; Ziegler, 2000) and Nampt has been found to be important for sustaining a number of reactions coordinated by these enzymes. This includes poly ADP-ribose polymerase (PARP)-mediated DNA repair (Rongvaux et al., 2008), SIRT1-mediated cell longevity (van der Veer et al., 2007), and SIRT3/4-mediated protection against apoptosis (Yang et al., 2007). Unlike these latter processes, cell migration has not been directly linked to NAD^+ turnover and a role for Nampt in motility has not previously been considered. However, in view of the upregulation of Nampt observed during patterned SMC migration, we questioned whether active generation of NAD^+ might underlie a control system for cell migration.

We report here that Nampt can drive highly efficient, directionally persistent cell migration. Using time-lapse microscopy, we found that Nampt activity regulated the size and protrusion rate of SMC lamellipodia. Moreover, Nampt activity effectively locked a small but highly protrusive lamellipodium in position. We also found that Nampt could localize to the lamellipodium itself, in a microtubule-dependent manner, and that its effects on polarity and lamellipodial stability were mediated by Cdc42 activation. The findings thus identify a novel, NAD^+-synthesis-dependent control mechanism for directed cell motility.

Results

Nampt regulates SMC patterning and directionally persistent SMC migration

We have found that withdrawing serum from cultures of HITC6 SMCs induces them to stream into clusters. This patterned motility response was associated with upregulation of Nampt (van der Veer et al., 2005). To determine whether Nampt activity was required for SMC patterning we subjected HITC6 SMCs to serum withdrawal in the presence or absence of 10 nM FK866, a non-competitive inhibitor of Nampt that, at this concentration, suppresses Nampt activity in SMCs to 20% of the baseline level (van der Veer et al., 2007). Whereas vehicle-treated SMCs were induced to elongate and stream toward sites of cell coalescence over 48 hours, FK866-incubated cells retained their random orientation without patterning (Fig. 1A, top). To determine whether increasing Nampt activity impacted cell streaming, SMCs were infected with a retrovirus containing human Nampt cDNA, which increases intracellular NAD^+ levels (van der Veer et al., 2005). Nampt- or vector-expressing SMCs were then subjected to partial serum withdrawal (3% FBS). Under these conditions, vector-infected SMCs underwent modest streaming. However, Nampt-overexpressing SMCs underwent striking cell alignment and pronounced streaming into clusters (Fig. 1A, bottom).

We next determined whether Nampt exerted control over the migration paths of individual cells not part of a collective. For this, SMCs were plated at low density (3000 cells/cm^2) in 10% FBS-supplemented medium and migration was tracked by time-lapse video microscopy. Vehicle-incubated SMCs under these conditions displayed exploratory migration. However, following inhibition of Nampt activity for 24 h with FK866, migration was even more disordered with frequent cell turning (Fig. 1B,C). In contrast, Nampt-overexpressing cells crawled with pronounced directional persistence, translocating up to 200 μm with little change in direction (Fig. 1B,C; supplementary material Movies 1, 2).

These effects of altered Nampt activity were quantified by assessing the ratio of net cell displacement (D) to total distance traveled (T). A D/T ratio of 1 denotes straight-line translocation, whereas smaller ratios indicate progressively less linear paths (Pankov et al., 2005). In FK866-exposed SMCs, D/T was 25% lower than that in control cells ($P=0.005$). In contrast, Nampt-overexpressing cells (Nampt-SMCs) displayed a 24% greater D/T than vector-expressing cells (vector-SMCs; Fig. 1D, $P=0.0001$). Overall cell migration speed was not significantly impacted by FK866 ($P=0.37$) although increased somewhat (1.18-fold) by Nampt overexpression ($P=0.004$). Because migration speed might impact D/T, we quantified the distribution of angles between each hourly translocation step to yield a turning index, or linear dispersion coefficient, which is a measure of directional stability that is independent of migration speed (Cantarella et al., 2009). This index was decreased by FK866 treatment ($P=0.001$) and increased by Nampt overexpression ($P=0.016$, Fig. 1D), further supporting a role for Nampt in straight-line motility.

Together, these findings reveal that human vascular SMCs have the capacity to undergo directional migration in the absence of an exogenously established chemotactic gradient, both as a collective and as individual cells. Moreover, the findings indicate that the salvage pathway for NAD^+ biosynthesis contributes to this innate directionality.

Nampt constrains lamellipodial size but drives lamellipodial protrusion

To investigate the mechanism by which Nampt promotes directional persistence, we evaluated specific features of the lamellipodium. In other cell types, random motility has been functionally linked to large, broad lamellipodia (Pankov et al., 2005). To determine if Nampt activity impacted lamellipodium morphology, we measured the edge length and radial dispersion of the leading lamellipodium. In SMCs exposed to FK866, mean lamellipodial length, measured as the length of ruffling cell edge relative to total cell perimeter, was significantly greater than that of vehicle-treated cells (1.2-fold, $P=0.009$). The lamellipodia were also broader (1.4-fold, $P=0.045$), assessed from the angle between two lines connecting the center of the nucleus to each end of the lamellipodium (Fig. 2A). Consistent with these differences, lamellipodia in Nampt-overexpressing SMCs had a significantly smaller edge length and significant smaller radial dispersion ($P=0.001$, $P=0.004$, respectively; Fig. 2A).

We next asked whether Nampt impacted lamellipodial protrusion itself. Rapid acquisition time-lapse microscopy revealed that Nampt imparted a striking change in lamellipodium movement. Rather than the back and forth protrusive/retraction activity of control SMCs there was a highly ‘fluid’ ruffling pattern in Nampt-SMCs with steady forward protrusion (Fig. 2B; supplementary material Movies 3, 4). Quantification of lamellipodium protrusion rate, from images every 30 seconds, revealed a 2.2-fold increase in protrusion rate in Nampt-overexpressing cells compared to vector-expressing cells ($P=0.012$, Fig. 2B). FK866 prevented the increase in protrusion rates observed in Nampt-SMCs. Thus, Nampt activity shrinks the lamellipodium but also drives its protrusion, a profile that, at least in part, could underlie the observed increases in migration speed and directional persistence.

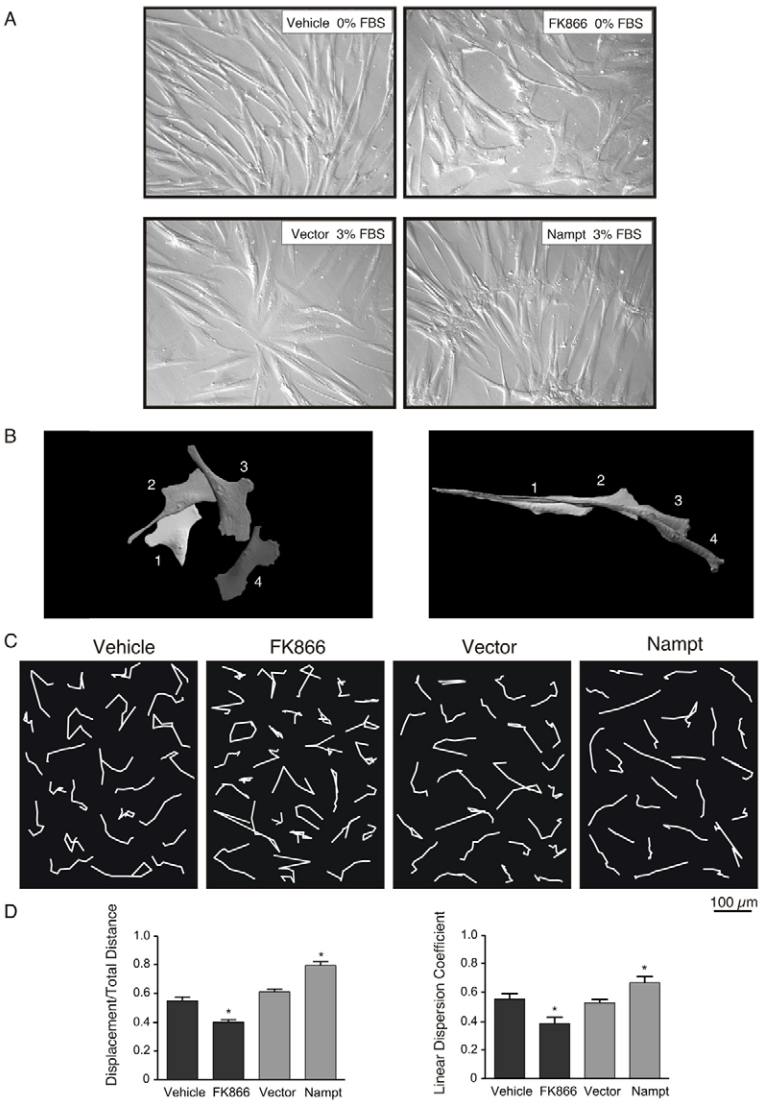

Fig. 1. Nampt stimulates directionally persistent migration. (**A**) Hoffman-modulated contrast images of HITC6 SMCs 48 hours after complete (top panel) or partial (bottom panel) serum withdrawal. Vector-SMCs subjected to serum withdrawal stream collectively into aggregates, following direct translocation pathways (top left). In contrast, cells incubated with the Nampt inhibitor, FK866 (10 nM), maintain their random orientation (top right). Vector-infected SMCs subjected to partial serum withdrawal show a moderate degree of streaming (bottom left). However, cells overexpressing Nampt display striking alignment and streaming (bottom right). (**B**) Migration paths of control (left) and Nampt-overexpressing (right) SMCs in 10% FBS that were plated at low density. Cells were traced at 0, 100, 220, 350 minutes for Vector-SMCs and 0, 100, 205, 380 minutes for Nampt-SMCs, and overlaid to display the migration paths. Corresponding videos can be seen in supplementary material Movies 1 and 2. (**C**) Migration paths of HITC6 SMCs migrating in medium supplemented with 10% FBS to promote otherwise non-directed migration. Individual migration paths of 25 SMCs per condition, over 8 hours, was ascertained by time-lapse microscopy and arranged on the black background. (**D**) Quantification of innate directional persistence over 8 hours, as determined by the ratio of net displacement over total distance traveled (D/T, left) and by the linear dispersion coefficient derived from the hourly mean angular vector change (right). Graph depicts the mean of 50–90 cells per condition. *$P=0.005$ versus vehicle, $P=0.0001$ versus vector-SMCs for D/T; $P=0.001$ versus vehicle or $P=0.016$ versus vector-SMCs.

Nampt constrains dynamic repositioning of the lamellipodium

Lamellipodial activity is characterized not only by short-term protrusive motion but also by longer-term repositioning around the cell periphery. For SMCs, we found that this typically entailed recruitment of previously non-ruffling plasma membrane on one end of the lamellipodium and termination of ruffling at the other end. Dispersion of ruffling at both ends was seen less frequently and was typically asymmetrical. To quantify this lamellipodial wandering phenomenon, time-lapse assessment over 8 hours was undertaken and the angular shifts between successive lines connecting the center of the nucleus to the mid-point of the lamellipodium were determined hourly. Using this index, the average lamellipodium repositioning rate in FK866-incubated SMCs was 42% higher than that in vehicle-treated SMCs ($P=0.003$; Fig. 2C). In contrast, the lamellipodium repositioning rate in Nampt-SMCs was 41% lower that vector-infected SMCs ($P<0.0001$). These findings established that Nampt imposed lateral restraint on lamellipodial dispersion, a previously undetected level of control over SMC motility.

Nampt drives bipolar elongation of SMCs

We next asked whether the observed lamellipodium anchoring phenomenon by Nampt might play a general role in regulating cell shape. An important SMC shape, in addition to the asymmetric unipolar morphology of migratory SMCs, is the symmetric bipolar morphology of contractile SMCs. *In vivo*, this is characterized by striking cell elongation of up to 200 μm (Peters et al., 1983), however, this morphology is generally not identified in culture. To assess SMC elongation, we tracked the immediate spreading patterns of low-density, trypsin-dispersed HITC6 SMCs. Control SMCs spread from their spherical morphology by ruffling and extending most of the adherent cell periphery. Ruffling then terminated at discrete regions to yield multiple, small lamellipodial extensions and a spread, multipolar morphology (Fig. 3; supplementary material Movie 5). In Nampt-expressing SMCs, the initial, diffuse ruffling pattern was similar to that of control SMCs. However the subsequent dissipation of ruffling was more extensive and followed a reproducible pattern whereby two co-dominant lamellipodia emerged at opposite ends of the cell. The position of these lamellipodia relative to the long axis of the cell

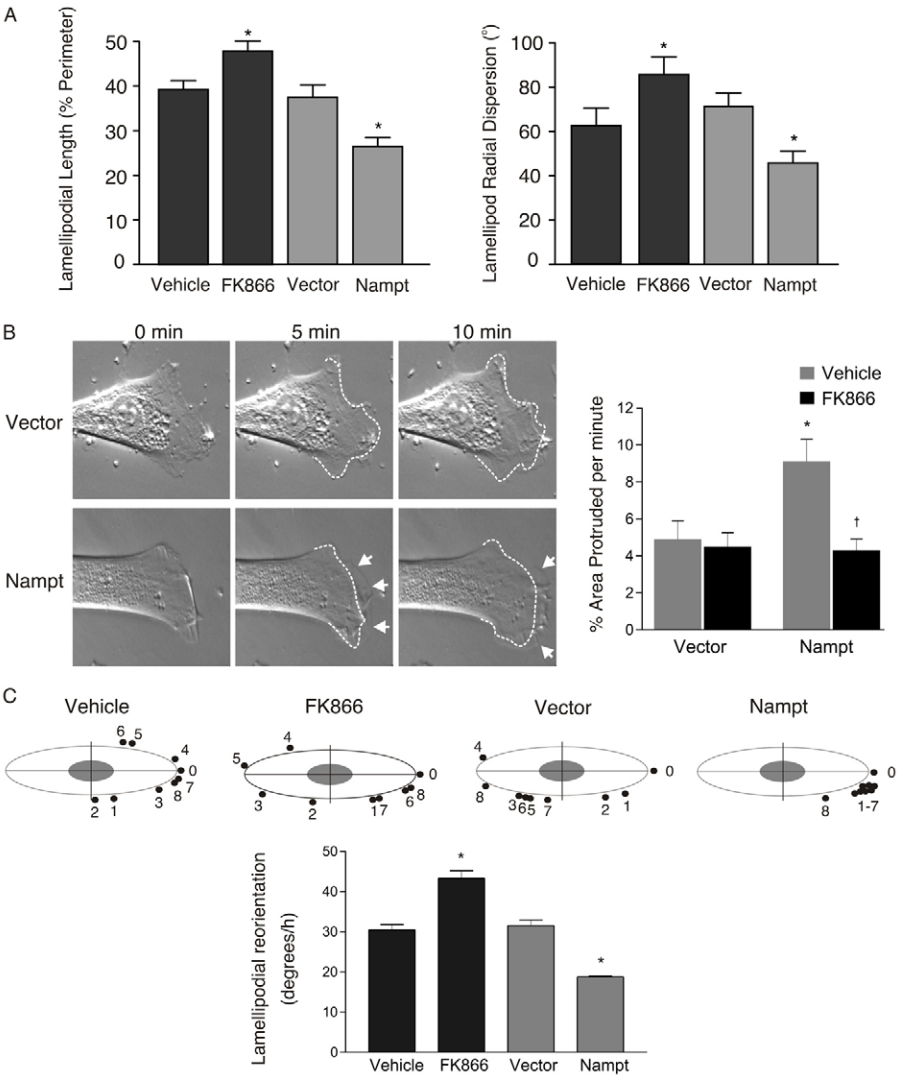

Fig. 2. Effect of Nampt on lamellipodial size, protrusion rate and dynamic repositioning. (**A**) Graphs depicting lamellipodial edge length (left) and radial dispersion (right) in HITC6 cells in the presence or absence of FK866 (10 nM) and in vector-SMCs and Nampt-SMCs; 35–55 cells per length condition, 45–75 cells per radial dispersion conditions. *P=0.009 versus vehicle, P=0.001 versus vector SMCs for length, P=0.045 versus vehicle, P=0.004 for radial dispersion. (**B**) Hoffman-modulated contrast images of vector and Nampt-infected SMCs illustrating lamellipodial protrusion over 10 minutes. SMCs were cultured in M199 with 10% FBS. The dashed white lines identify the position of the leading edge 5 minutes before the image was taken. Arrows denote forward protrusions. Time-lapse movies of the illustrated cells are in the supplementary material Movies 3 and 4. On the right is a graph depicting lamellipodial protrusion rates for vector- and Nampt-expressing SMCs with and without FK866 (10 nM), determined as the average forward displacement of the cell per minute, expressed relative to the total cell area; 15 cells per condition. *P=0.012 versus Vector-SMCs incubated with vehicle, †P=0.001 versus Nampt-SMCs incubated with vehicle. (**C**) Schematic depiction of the lamellipodium position of representative cells subjected to Nampt inhibition (FK866) or enhancement (Nampt overexpression) and their respective control cells, over 8 hours. The relative location of the mid-point of the lamellipodium, at hourly intervals, is depicted by the black dots. Below is a graph depicting the repositioning of the dominant lamellipodium for a given cell over 8 hours. 40–55 cells per condition. *P=0.003 versus vehicle, P<0.0001 versus vector-SMCs.

remained constant and as they protruded the lamellipodia progressively narrowed to form non-ruffling ‘points’ at either end of a strikingly elongated cell (Fig. 3; supplementary material Movie 6). Serial tracking of aspect (length–width) ratios revealed a 16-fold increase in aspect ratio of Nampt-SMCs over 8 hours. This was 2.3-fold higher than that of vector-SMCs (aspect ratio 6.9, P=0.008). The 8-hour aspect ratio of Nampt-SMCs incubated with 5 nM FK866 was significantly lower than that for Nampt-SMCs (P=0.015) and similar to that of vector-SMCs. Taken with the migration data, these findings indicate that Nampt activity underlies a process for constraining the size, position and activity of lamellipodia in a manner that, depending on the prevailing conditions, can optimize both directional migration and cellular elongation.

Nampt is compartmentalized to lamellipodial protrusions

A general cellular pool of NAD^+ has previously been assumed, however, emerging data suggest that NAD^+-dependent pathways are in fact compartmentalized (Nikiforov et al., 2011). This compartmentation arises in part from spatial segregation of NAD^+ biosynthetic enzymes (Berger et al., 2005; Koch-Nolte et al., 2011). Using western blot analysis of subcellular fractions of human SMCs, we found that Nampt localized to the cytoplasm and nucleus, with most found in the cytoplasm (not shown; Fig. 4A). Interestingly, Nampt was also present in a plasma-membrane-enriched fraction characterized by the presence of Na^+/K^+ ATPase with little to no α-tubulin (Fig. 4B). Because Nampt does not have features of a membrane-spanning or membrane-integral protein (Khan et al., 2006), we reasoned its presence in this subfraction might reflect cytosolic Nampt close to the inner leaflet of the plasma membrane. Consistent with this possibility, immunostaining SMCs for Nampt revealed signal at the cell edge and particularly at sites of lamellipodium ruffling, in addition to more diffuse intracellular signals (Fig. 4C).

To further assess the possibility that Nampt localized in the lamellipodium, SMCs were transduced with retrovirus containing cDNA for either Nampt–eGFP or eGFP alone and imaged using time-lapse fluorescence microscopy. This revealed pronounced Nampt signal at the protrusive lamellipodium (Fig. 4D; supplementary material Movies 7, 8). Interestingly, vesicular flow of Nampt–eGFP out of the lamellipodium was also observed, suggesting a retrograde Nampt transport system.

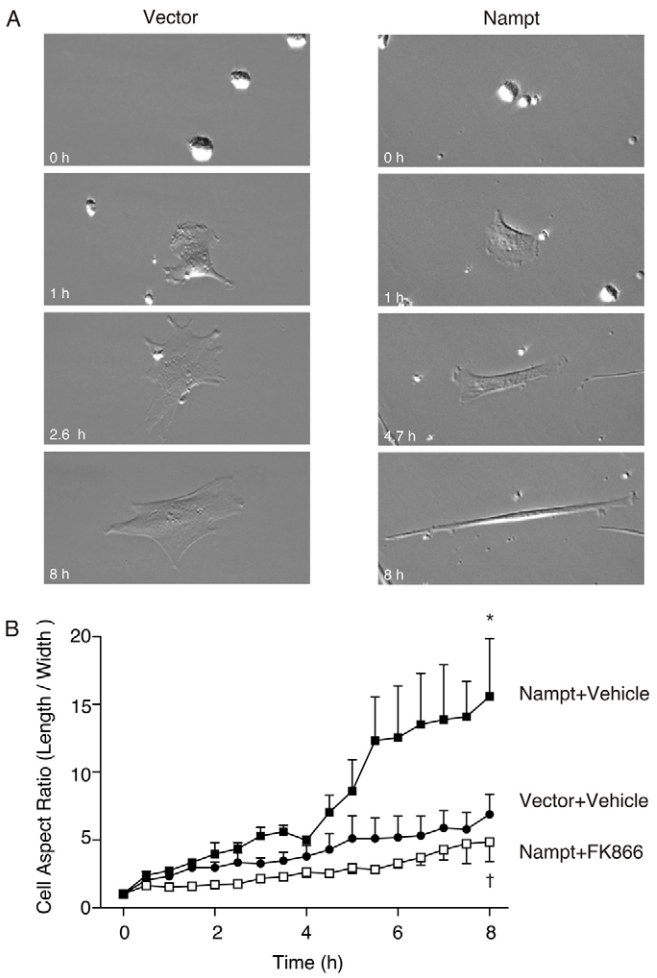

Fig. 3. Effect of Nampt on SMC elongation and acquisition of bipolarity. (**A**) Hoffman-modulated contrast images of human SMCs infected with retrovirus containing cDNA for vector (left) or Nampt (right). SMCs were detached with trypsin-EDTA, resuspended in M199 containing 3% FBS, and plated at low density. Images have been cropped from the video frames and repositioned to facilitate visualization of cell shape changes, maintaining identical magnifications. Time-lapse movies of the full fields of view can be found in the supplementary material Movies 5 and 6. (**B**) Graph depicting the aspect ratios of vector-infected and Nampt-overexpressing SMCs in the presence or absence of 5 nM FK866. SMCs were acutely plated in M199 with 3% FBS. Data represent 8–15 cells per condition. *P=0.008 versus vector-SMCs with vehicle, $^{\dagger}P$=0.015 versus Nampt-SMCs with vehicle.

To determine whether Nampt was actively transported to the lamellipodium, we evaluated fluorescence recovery after photobleaching (FRAP) in the presence of specific transport inhibitors. Re-accumulation of fluorescence for 60 seconds after photobleaching was quantified. Fluorescence recovery in SMCs incubated with nocodazole to trigger tubulin depolymerization was notably blunted, with a time-fluorescence integral (TFI) 67.2% of that of control SMCs (P=0.001; Fig. 5). TFI in SMCs incubated with the microtubule stabilizer, paclitaxel, was also significantly lower than vehicle-treated Nampt–eGFP SMCs (P=0.02). The fluorescence recovery half-times for Nampt–eGFP were also significantly lengthened by nocodazole (P=0.028) and paclitaxel (P=0.030). Interestingly, paclitaxel-incubated SMCs showed augmented accumulation of Nampt at lamellipodial protrusions, suggesting either bolus delivery of Nampt to the leading edge from acutely stabilized microtubules or a microtubule instability-based mechanism for removing Nampt from the lamellipodium. Incubation of SMCs with brefeldin A to inhibit protein transport through the endoplasmic reticulum–Golgi complex had no effect on Nampt localization in the lamellipodium and no impact on the accumulation rate after photobleaching. Collectively, these data indicate that Nampt is compartmentalized in SMCs and can be localized, in a microtubule-dependent fashion, in lamellipodial protrusions.

Nampt activates Cdc42

Rho family GTPases are essential for lamellipodial protrusion. Furthermore, suppression of Rac1 activity has been implicated in directionally persistent migration (Pankov et al., 2005). Because of this, and the strong relationship we observed between Nampt and the lamellipodium, we sought to determine if there was a relationship between Nampt and Rac1. We first assessed this in HITC6 SMCs subjected to serum withdrawal. With extended serum-free conditions HIT SMCs stop proliferating but remain healthy with reduced apoptosis rates (Li et al., 2001; Li et al., 1999). Over 6 days following serum withdrawal, there was marked (2.9-fold) upregulation of Nampt expression, together with progressive shrinkage of lamellipodia (Fig. 6A). Surprisingly, this was not associated with a decline in expression or activity of Rac1. However, there was a 3.6-fold increase in Cdc42 activity within 4 days of serum withdrawal. Consistent with these findings, inhibiting Nampt activity with FK866 had no effect on basal Rac1 activity but, instead, significantly reduced Cdc42 activity (Fig. 6B). In addition, overexpression of Nampt increased Cdc42 activity and modestly increased Rac1 activity.

We next investigated whether Nampt and Cdc42 colocalized in the cell. Immunoprecipitation of Cdc42 followed by immunoblotting for Nampt did not yield a detectable signal, nor was a signal detected following Nampt immunoprecipitation and Cdc42 immunoblotting (data not shown). However, affinity precipitation of active, GTP–Cdc42/Rac1 did reveal an immunodetectable Nampt signal, albeit relatively weak, indicating an association between the active Rho GTPase and endogenous Nampt (Fig. 6C).

To confirm an association between Nampt and Cdc42 specifically, and determine if this was spatially localized, we undertook an *in situ* colocalization assessment using a proximity ligation approach that identifies designated proteins residing within 40 nm of each other (Söderberg et al., 2006). There was little to no proximity signal in cells incubated with the anti-Cdc42 antibody alone, or the anti-Nampt antibody alone (Fig. 6E, left). However, cells immunolabeled with both antibodies displayed amplification signals, indicating that a proportion of Cdc42 colocalized with Nampt (Fig. 6E, middle). Colocalization signals were not extensive, but were increased significantly in SMCs overexpressing Nampt (Fig. 6F). Moreover, upon knockdown of Cdc42 abundance by siRNA, the proximity signals were substantially reduced (Fig. 6E, right; Fig. 6F). Interestingly, Nampt–Cdc42 colocalization signals were enriched in cell protrusions. Together, these data indicate that Nampt can both interact with and activate Cdc42 in SMCs and that a Nampt-Cdc42 association is particularly evident in lamellipodial protrusions.

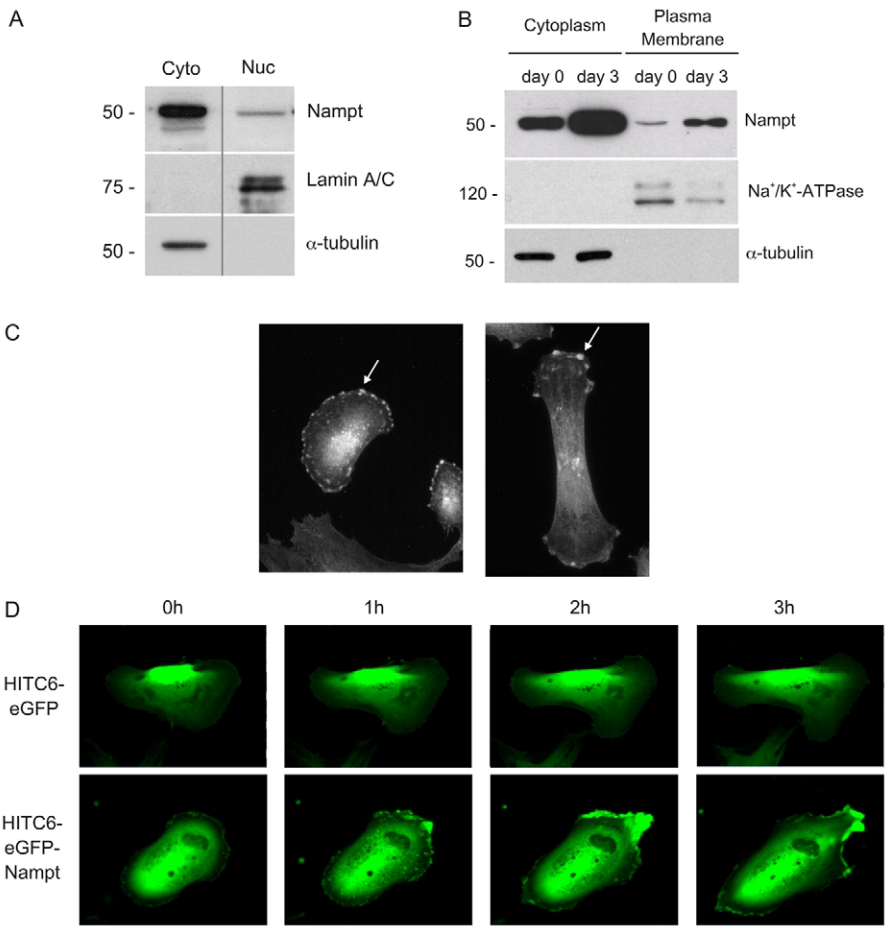

Fig. 4. Nampt localizes to a lamellipodium compartment. (**A**) Western blots showing relative abundance of Nampt in the cytoplasmic and nuclear fractions of human SMCs. The nuclear fraction is characterized by the presence of lamin A/C and absence of α-tubulin. The vertical line between lanes denotes repositioned lanes from the same blot for side-by-side comparison. (**B**) Western blots showing presence of Nampt in a plasma-membrane-enriched fraction, indicated by the presence of Na^+/K^+-ATPase. Nampt abundance increases 3 days after serum withdrawal. (**C**) Photomicrographs of SMCs immunostained for Nampt showing signal (arrows) at lamellipodia of early spreading (left) and elongating (right) SMCs. (**D**) Hourly micrographs of migrating SMCs stably expressing either eGFP or Nampt–eGFP showing pronounced accumulation of Nampt–eGFP at the protrusive lamellipodium. Corresponding movies, which also suggested retrograde vesicular transport of Nampt–eGFP, can be seen in supplementary material Movies 7 and 8.

Nampt-regulated directional stability is mediated by Cdc42

We next determined whether Nampt-induced directional stability required Cdc42. SMCs stably infected with retrovirus containing cDNA for Nampt or vector alone were subjected to Cdc42 knockdown by electroporating siRNA (Nucleofector), which reduced Cdc42 expression by ~70% (Fig. 7A). Vector-SMCs containing control siRNA and vector SMCs subjected to Cdc42 knockdown both displayed broad lamellipodia (Fig. 7B, top). However in Nampt-overexpressing SMCs subjected to Cdc42 depletion, the lamellipodium configuration was atypical, with prominent side protrusions emanating from the edge of the parent lamellipodium, sometimes giving rise to a tripolar appearance to the cell (Fig. 7B, bottom right). These findings suggest that Cdc42 knockdown abrogated Nampt-induced positional restraint of lamellipodia, but not the protrusive actions of Nampt.

Quantitative cell movement assessment revealed that the D/T ratio and linear dispersion (turning) coefficient was increased in Nampt-SMCs exposed to control siRNA, but this increase in directional persistence did not occur in Nampt-SMCs subjected to Cdc42 knockdown (Fig. 7C,D). Furthermore, Nampt-SMCs exposed to control siRNA showed restricted lamellipodium reorientation around the cell periphery, compared to vector-SMCs, but this was not observed in Nampt-overexpressing cells subjected to Cdc42 knockdown (Fig. 7E).

Collectively, these findings indicate that activation of Cdc42 is a downstream consequence of Nampt-mediated NAD^+ biosynthesis in SMCs and mediates Nampt-driven stabilization of lamellipodium position.

Discussion

The ability of cells to maintain their direction of crawling has implications for tissue development, repair and stabilization. This study established that human vascular SMCs have the capacity to engage in directionally persistent migration, independent of external guidance cues, and that this productive mode of migration is orchestrated by NAD^+ biosynthesis. The existence of a NAD^+-based control system was revealed by pronounced changes in the spreading and crawling behavior of cells upon altering the abundance or activity of Nampt. Originally described as a cytokine that may be involved in B cell development or glucose uptake, Nampt is, in fact, an enzyme that catalyzes the rate-limiting step in the NAD^+ salvage reaction from nicotinamide (Revollo et al., 2004; van der Veer et al., 2005). We determined that this enzyme imparted directionality to migrating SMCs by generating protrusive lamellipodia that were restricted in size and anchored in position.

Whereas external guidance cues dictate where a cell crawls, the stability with which the cell directionally translocates is determined by intrinsic steering mechanisms. Known determinants of intrinsically directed migration include the cell polarity machinery, integrin trafficking, calcium signals, the extracellular matrix architecture, and Rho GTPases (Moissoglu

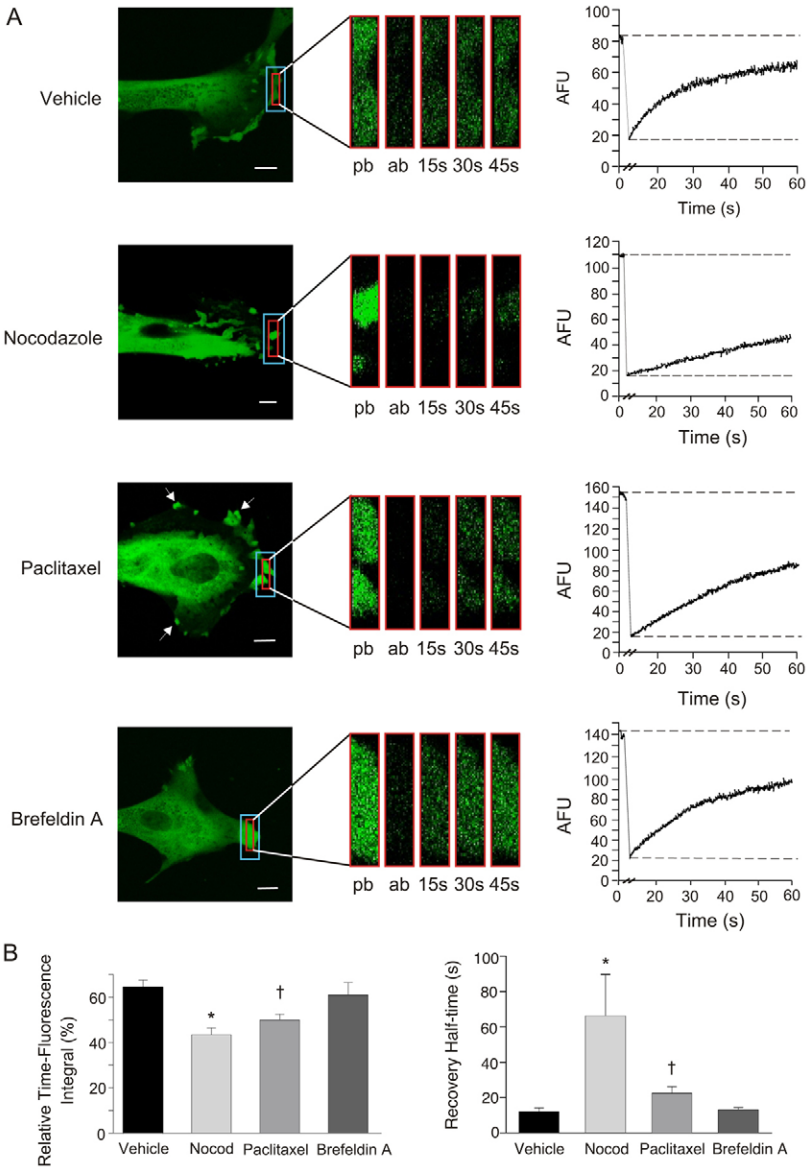

Fig. 5. Nampt is transported to the leading edge of SMCs. (**A**) Confocal microscope images of SMCs expressing Nampt–eGFP subjected to photobleaching of the lamellipodium Nampt signal. The outer bleached and inner recovery assessment zones are depicted. The frames adjacent to each cell depict the pre-bleach (pb), after-bleach (ab) and recovery signals. Quantitative data is depicted in the adjacent graph. Cells were pre-incubated for 1 hour with vehicle (n=9), nocodazole (n=9), paclitaxel (n=9) or brefeldin A (n=5). Arrowheads indicate Nampt signal accentuation following cell exposure to paclitaxel. (**B**) Graphs of fluorescence recovery denoted as the time-fluorescence integral expressed relative to integrated 60-second signal without photobleaching (left) and recovery half-time (right). *P=0.001, $^{\dagger}P$=0.02 versus vehicle for time-fluorescence integral; *P=0.028, $^{\dagger}P$=0.030 versus vehicle for recovery half-time.

and Schwartz, 2006; Petrie et al., 2009). NAD^+ regulation thus constitutes a new participant in the control of directional motility, and one that we determined was relevant to SMCs migrating into a collective as well as individually migrating cells. The observation that lamellipodial dynamics were regulated by Nampt is in keeping with the centrality of the lamellipodium in defining cell translocation patterns. Directionally persistent migration has been found to be inversely related to the size of the lamellipodium (Pankov et al., 2005) and, consistent with this, Nampt expression led to lamellipodial shrinkage and Nampt inhibition yielded broad lamellipodia. Nampt also restrained lateral shifting of the lamellipodium and effectively locked the lamellipodium in a single position thereby limiting cell turning. Interestingly, these restrictive actions on the lamellipodium were not associated with reduced membrane protrusion but in fact enhanced protrusive activity. Thus, Nampt acts as an orchestrator of lamellipodial behavior that coordinately regulates its size, position, and protrusion to drive efficient migration.

We also identified that generation of anchored and protrusive lamellipodia by Nampt did not exclusively impact migration but also enabled acutely spreading SMCs to undergo bipolar elongation. SMCs can assume unipolar and bipolar morphologies, with each morphology being tightly linked to different functions. Elongated, bipolar SMCs are central to the contractile behavior of well-differentiated SMCs and we have previously shown that Nampt promotes upregulation of SMC contractile genes (van der Veer et al., 2005). The current studies establish, however, that Nampt is not deterministic for either a contractile or migratory SMC phenotype. Rather, Nampt activity serves to optimize the morphological patterning required of either phenotype, by effectively locking in polarity and driving stable protrusions. Because cell shape dictates cell behavior (Thakar et al., 2009), this morphology stabilizing effect could serve as a mechanism to optimize various cell functions.

The observation that Nampt was transported to the leading edge of the cell implicates locally generated NAD^+ in

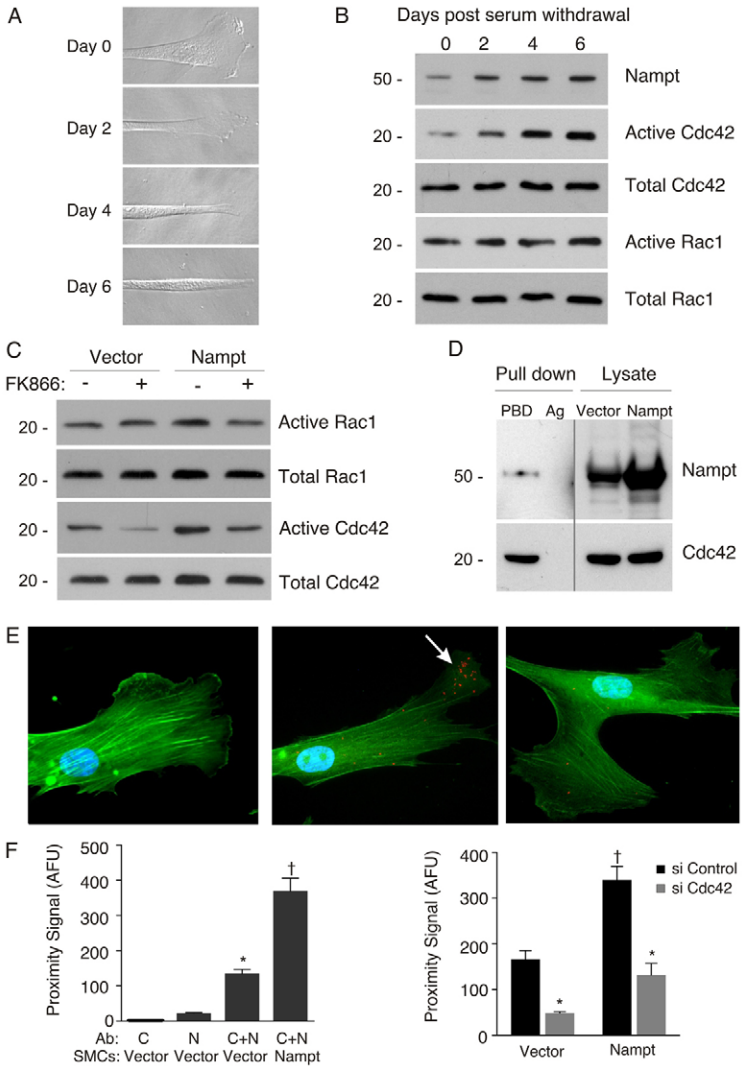

Fig. 6. Activation of Cdc42 by, and association with, Nampt. (**A**) Hoffman-modulated contrast images of the leading aspect of HITC6 SMCs before (day 0) and at designated times after withdrawal of serum from the cultures. Progressive shrinkage of the lamellipodia can be seen. (**B**) Western blots of Nampt and total and active GTP-bound Rac1 and Cdc42 in HITC6 SMCs subjected to serum withdrawal. (**C**) Western blots showing total and active GTP-bound Rac1 and Cdc42 in vector-infected or Nampt-overexpressing SMCs in the presence or absence of FK866. (**D**) Immunoblot of Nampt following affinity pulldown of active, GTP-bound Cdc42/Rac1. PBD, Pak1 p21-binding domain; Ag, agarose. Nampt immunoblot of whole cell lysates from vector-SMCs and Nampt-SMCs that were simultaneously run and probed are shown on right. Lysates constituted 5% of the total protein from which Cdc42–GTP was precipitated, and the Nampt bands were developed using a shorter exposure than that for the affinity precipitated Nampt fraction. The vertical line separates lanes subjected to different exposure and placed side-by-side for comparison. (**E**) Fluorescence micrographs of SMCs subjected to proximity ligation assay for Nampt and Cdc42. Proximity amplification signals appear red, actin microfilament bundles were labeled with FITC–phalloidin (green), and nuclei were stained with Hoechst 33298. Cells shown depict: control conditions using the anti-Cdc42 antibody alone (left); experimental conditions using both anti-Cdc42 and anti-Nampt antibodies (middle); experimental conditions following Cdc42 knockdown with siRNA (right). Punctate amplification signals are enriched at the lamellipodium (arrow). (**F**) Graphs depicting amplification signal intensities, derived from at least 150 cells/condition. AFU, arbitrary fluorescence units; Ab, antibody; C, anti-Cdc42; N, anti-Nampt. *$P<0.001$ versus corresponding controls. $^{\dagger}P<0.001$ versus vector.

lamellipodial dynamics. Although NAD^+ and its precursors are small and potentially diffusible molecules, emerging evidence indicates there are distinct pools of NAD^+ generation in the cell, with an associated compartmentation of NAD^+-based signaling (Berger et al., 2005; Koch-Nolte et al., 2011). We identified Nampt in both cytoplasmic and nuclear fractions of SMCs, which is consistent with findings in other cell types (Kitani et al., 2003; Yang et al., 2007). However, cytoplasmic Nampt was not diffusely distributed but was polarized and prominent at membrane ruffles. This conclusion was based on: (1) immunostaining for endogenous Nampt; (2) the presence of Nampt in the plasma-membrane-enriched cell fraction; and (3) visualizing Nampt–eGFP in SMC lamellipodia by time-lapse microscopy. We cannot exclude the possibility that part of the ruffling-associated Nampt–eGFP signal arose from increased fluorescence signal generated by protrusions folding into the imaging light path. However, FRAP analysis revealed microtubule-dependent recovery of Nampt signal at the leading edge, implicating a regulated transport system. The relative hyperconcentration of Nampt–eGFP in protrusions observed after stabilizing microtubules with paclitaxel, as well as retrograde movement of Nampt–eGFP from the leading edge, further indicate a process of Nampt flux in and out of the lamellipodium. Interestingly, Nampt has recently been found to localize to myo-endothelial junctions, sites of opposed cellular protrusions of vascular smooth muscle cells and endothelial cells (Heberlein et al., 2012). Furthermore, this study found that Nampt strongly associates with microtubules *in vitro*. Taken together with our data, the findings suggest a microtubule-based transport system for the polarized delivery of Nampt to membrane protrusions. We speculate, therefore, that both the actions of Nampt at lamellipodia and the Nampt transport machinery itself, may determine the fidelity of motility.

Nampt was found to mediate its control over lamellipodia through Rho GTPases. Within this family, Rac1 is well known to promote the formation of broad lamellipodia, and data in fibroblasts and epithelial cells have revealed an inverse relationship between Rac1 activity and directional migration (Pankov et al., 2005). However, in contrast to our prediction based on these data, we did not find that Nampt suppressed Rac1 activity. Instead, we identified a strong relationship between Nampt-induced directionality and Cdc42. Cdc42 was activated in association with Nampt upregulation and lamellipodial shrinkage upon serum withdrawal. Likewise, Cdc42 was activated

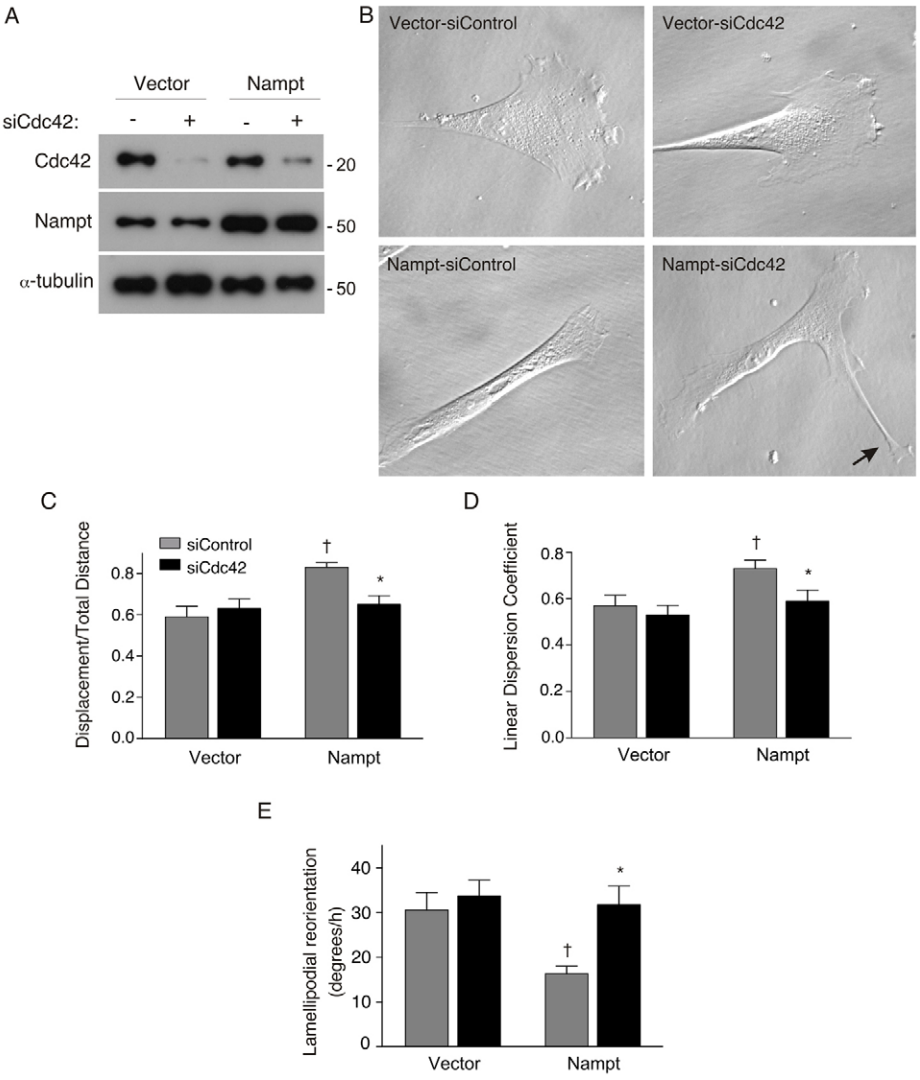

Fig. 7. Role of Cdc42 in Nampt-mediated directional migration. (**A**) Western blots depicting siRNA-mediated knockdown of Cdc42 in HITC6 SMCs stably transduced with retrovirus containing vector or cDNA encoding Nampt. (**B**) Hoffman modulated contrast images of vector-SMCs (top) or Nampt-SMCs (bottom) subjected to electroporation with control siRNA or Cdc42 siRNA. Side-protrusion is denoted by arrows. (**C–E**) Graphs depicting the effects of siRNA-mediated knockdown of Cdc42 on D/T of migration (C), linear dispersion coefficient (D) and dynamic repositioning of lamellipodia (E) over 8 hours. Cells were evaluated 48 hours after delivery of siRNA reagents; 25–40 cells per condition. $*P<0.0001$ versus Nampt-SMCs with control siRNA, $^{\dagger}P=0.001$ versus vector-SMCs with siRNA for D/T; $*P=0.008$ versus Nampt-SMCs with control siRNA, $^{\dagger}P=0.029$ versus vector-SMCs with siRNA for linear dispersion coefficient; $*P=0.002$ versus Nampt-SMCs with control siRNA. $^{\dagger}P=0.001$ versus vector-SMCs with control siRNA for lamellipodia reorientation.

following Nampt overexpression and Cdc42 activity was suppressed by FK866. We also identified that a proportion of Cdc42 was associated with Nampt, using both cell lysate and *in situ* colocalization approaches. The relatively low intensity of the association signal could reflect weak or transient complexes, but the lamellipodium-enriched association nonetheless identifies a novel interplay between the NAD biosynthesis machinery and at least one Rho GTPase. Furthermore, Cdc42 was required for Nampt-induced directionally persistent migration, as quantified by D/T ratio, the cell turning/linear dispersion coefficient, and dynamic repositioning of the lamellipodium. These findings are consistent with an established role for Cdc42 as a master regulator of front–rear polarity (Etienne-Manneville and Hall, 2001). Interestingly, Nampt overexpression also induced modest activation of Rac1, which could be due to Nampt expression per se or a downstream consequence of Cdc42 activation (Nishimura et al., 2005). Regardless, the specific balance of Cdc42 and Rac1 activities generated by Nampt may, in part, underlie the particular lamellipodial patterns observed.

The specific molecular cascades linking local NAD^+ biosynthesis and Cdc42 activity, or other mediators of cell polarization and lamellipodium dynamics, remain to be established, but members of the NAD^+-consuming families of enzymes are important candidates. Sirtuins and ARTs consume NAD^+ through deacetylation or ADP-ribosyltransferase reactions and there are extranuclear members of both families (Imai and Guarente, 2010; Smith, 2001) that might contribute to NAD^+ consumption at the lamellipodium. Another class of NAD^+-degrading enzymes is NADases, which generate the calcium signaling molecules ADP-ribose, cyclic ADP-ribose and NAADP (Koch-Nolte et al., 2011; Lee, 2004). Control of calcium flux is vital for cell migration (Espinosa-Tanguma et al., 2011) and it is noteworthy that high-calcium microdomains in the lamellipodium have been identified as critical for cell steering (Wei et al., 2009). Another potentially relevant consequence of local NAD^+ generation is regulation of cell adhesion. Focal-adhesion-related mechanosensing has been identified as a basis for fibroblast polarization (Prager-Khoutorsky et al., 2011) and it has been shown in zebrafish that NAD^+ production is required for cell adhesion to extracellular matrix and for localization of the focal adhesion complex adapter protein, paxillin (Goody et al., 2010). These possibilities warrant future investigation and we speculate

that a range of NAD^+-consuming reactions participate in cell polarization and lamellipodium dynamics, making the machinery for NAD^+ regeneration a crucial gateway.

In summary, we have identified an NAD^+-synthesis-dependent control mechanism for directionally persistent cell motility, and have established Nampt as a novel upstream regulator of Cdc42. Because Nampt is not an invariantly expressed enzyme and its activity can decline with aging (Costford et al., 2010; van der Veer et al., 2007), strategies to optimize NAD^+ biosynthesis could underlie new approaches for optimizing tissue repair and regeneration.

Materials and Methods

Cell culture and reagents

Experiments were performed using HITC6 SMCs, a non-immortal human SMC line isolated from the human internal thoracic artery (Li et al., 2001; Li et al., 1999). SMCs were cultured in M199 (Gibco/BRL) with the designated concentration of fetal bovine serum (FBS). Human SMCs stably expressing Nampt or eGFP-tagged Nampt (derived from pEGFP-C2; Clontech, Mountain View, CA) were generated using retrovirus, as previously described (Rocnik et al., 2002; van der Veer et al., 2005). Briefly, full-length cDNA in pQCXIP-IRES-PURO was transfected using calcium phosphate into the Phoenix-amphotropic retrovirus packaging cell line (kindly provided by Dr G Nolan, Stanford University Medical School, CA, distributed by ATCC, Manassas, VA). The retrovirus-containing supernatant was added to proliferating SMCs and stable transductants were selected with 3 μg/ml puromycin for 48 hours. Overexpression of Nampt was confirmed before each experiment by western blot analysis. FK866 was obtained from the National Institute of Mental Health, Chemical Synthesis and Drug Supply Program.

SMC migration and elongation

Motility of SMCs plated at 3500 cells/cm^2 was assessed by time-lapse microscopy, as described previously (Fera et al., 2004). Imaging was undertaken using a Zeiss inverted microscope (Axiovert S100) with Hoffman-modulated contrast optics and CCD camera (Cooled QICAM 12-bit Mono Fast 1394, QImaging Inc.) or a Leica DMI6000 B microscope with IMC optics and Leica DFC420 C camera. Images were acquired every 5 minutes over 8–12 hours using time-lapse software (Northern Eclipse Imaging software, Empix Inc. and Leica Application Suite). Ambient temperature was maintained at 37℃ with a temperature control cell (CC-100; 20/20 Technology Inc. or LiveCell, Pathology Devices) and cells were incubated in bicarbonate-reduced M199 with Hanks' salts and 25 mM Hepes. Cell migration speed was calculated as the sum of the hourly centroid translocations divided by the total imaging period. Directional persistence was determined as: (1) the ratio of the displacement (D) from a start position to the total distance (T) traveled (D/T) (Pankov et al., 2005); and (2) the turning index, or linear dispersion coefficient, an index of the distribution of the angles between each translocation step that is independent of cell migration speed (Cantarella et al., 2009). SMC elongation was determined in dispersed cells seeded at below 4000 cells/cm^2 in M199 with 3% FBS and immediately tracked. The lengths and widths of each cell in the field of view (10× objective) were quantified every 30 minutes.

Lamellipodium morphology, protrusion rate and dynamic repositioning

Lamellipodium morphology was determined in two ways. First, the length of the lamellipodium was measured by tracing and expressing this relative to the cell perimeter. Second, the spread or radial dispersion of the lamellipodium was determined as the angle between two lines connecting the center of the nucleus to each end of the lamellipodium. Lamellipodial protrusion rate was determined by acquiring images every 30 seconds over a 10-minute period. Each image was traced and sequential, paired images were digitally overlaid and subjected to Boolean subtraction to yield the area of plasma membrane that had protruded during each 30-second interval. This area of protrusion was expressed as a fraction of total cell area. The 30-second protrusion values taken over the course of an experiment were averaged and expressed as the mean fractional protrusion rate (% area/minutes). Dynamic repositioning of lamellipodia around the cell perimeter was assessed by identifying the mid-point of the lamellipodia every hour for 8 hours. A line intersecting the center of the nucleus and the lamellipodium mid-point was drawn and lamellipodium repositioning was measured based on the hourly angular deviation of this line, assessed in serial images. In order to specifically measure positional shifts in lamellipodium/ruffling with respect to the cell perimeter, deviations were only measured if the cell itself did not execute a turn, defined as a change in orientation of the nucleus by greater that 20°. If a cell did turn, a lamellipodium repositioning measurement was not recorded for that hourly interval.

Subcellular assessment and western blot analyses

Nuclear and cytoplasmic proteins were separated by step-wise lysis using NE-PER Nuclear and Cytoplasmic Extraction Reagents (Thermo Fisher Scientific, Nepean, Canada). Plasma membrane and cytoplasmic fractions were also harvested using sucrose gradient centrifugation. Briefly, SMCs in sucrose-HEPES buffer (SHB, 20 mM HEPES, 1 mM EDTA, 255 mM sucrose, pH 7.5) containing protease inhibitors (Protease Inhibitors Cocktail and Phosphatase Inhibitor Cocktail 2; Sigma, Oakville, Canada) and phenylmethanesulfonyl fluoride (1 mM; Sigma) were homogenized and subjected to centrifugation at 1000 ***g*** for 15 minutes. The supernatant was subjected to centrifugation at 16,000 ***g*** for 20 minutes yielding a supernatant of cytoplasm and pellet, which was resuspended in SHB and layered onto a sucrose cushion (30% sucrose in PBS) and spun at 53,000 ***g*** for 35 minutes in a Beckman ultracentrifuge using a TLA120.1 rotor. The plasma membrane fraction was collected from the SHB-sucrose cushion interface.

For western blot analysis, proteins were resolved on SDS-polyacrylamide gels, transferred to PVDF membranes (Millipore, Billerica, MA) and Nampt was detected using a polyclonal rabbit antibody against human PBEF/Nampt (1:3000; Bethyl Laboratories, Montgomery, TX). Fractions were probed using a polyclonal antibody against lamin A/C (1:2000; Santa Cruz Technologies, Santa Cruz, CA) and monoclonal antibodies against Na^+/K^+-ATPase (1:1000; Santa Cruz Biotechnologies) and α-tubulin (clone B-5-1-2; 1:25,000; Sigma) to assess nuclear, membrane, and cytoplasmic fractions, respectively. Secondary antibodies were horseradish-peroxidase-conjugated anti-rabbit and anti-mouse IgG (GE Healthcare, Baie d'Urfe, Canada) and signals were detected with SuperSignal West Pico Chemiluminescent Substrate (Thermo Fisher Scientific) and exposed on Amersham Hyperfilm (GE Healthcare). Bands were quantified by laser scanning densitometry (GS-700 Imaging Densitometer; Bio-Rad).

Immunostaining

SMCs grown on glass coverslips were fixed for 20 minutes with 4% paraformaldehyde, permeabilized for 20 minutes with 0.2% Triton X-100, and incubated with rabbit anti-PBEF/Nampt (Bethyl; 1:300) for 1 hour in 5% normal goat serum. Bound primary antibody was detected with an Alexa-Fluor-488-labeled goat-anti-rabbit IgG (1:500; Molecular Probes, Eugene, OR). Nuclei were stained with 2.5 μg/ml Hoechst 33258 and coverslips were mounted with PermaFluor (Thermo Fisher Scientific). Cells were visualized using an Olympus BX50 microscope with a BX-FLA illuminator, UPlanF1 objective lenses, cooled Retiga EXi Mono Fast 1394 camera (QImaging Inc.), and Northern Eclipse image analysis software.

Confocal microscopy and fluorescence recovery after photobleaching

SMCs stably expressing EGFP or EGFP-tagged Nampt plated on glass-bottomed dishes were incubated with vehicle (DMSO, 0.1% v/v), nocodazole (1 μM; Sigma), paclitaxel (1 μM; Sigma), or brefeldin A (5 μg/ml; Sigma) 1 h prior to analysis. Confocal microscopic analysis of lamellipodial Nampt was undertaken using a Zeiss laser scanning microscope 510Meta and a Plan-Apochromat 63×/1.4 NA oil DIC objective. Cells were maintained at 37℃ using a bionomic controller (20/20 Technology, Mississauga, Ontario). Fluorophore excitation was achieved using an argon/2 laser unit. Lamellipodium signal was bleached using a rectangular region of interest and fluorescence recovery was probed in a rectangular subregion that constituted 16% of the bleached zone. Bleaching was undertaken at 488 nm with full intensity for 6 seconds with 50 scans. Baseline fluorescence intensity was established from 10 pre-bleach scans and fluorescence recovery assessed in 500 post-bleach scans, at 123 mseconds/scan. Fluorescence recovery was assessed over 60 seconds and quantified as the time–fluorescence integral and as the recovery half-time, the latter using one-phase association curve fitting (Graphpad Prism 5).

Rho GTPase activity and function

The activity of Rac1 and Cdc42 in SMCs were assayed from lysates that were affinity purified using a fragment of p21-activated kinase 1 (PAK1) expressed as a fusion protein with glutathione *S*-transferase, as previously described (Fera et al., 2004; Leung et al., 2004). Affinity-precipitated proteins were separated on 15% SDS-PAGE as were parallel lysates not subjected to affinity precipitation. Proteins were transferred to PVDF membranes and immunoblotted with primary antibodies against Rac1 (R56220, BD Biosciences, Mississauga, Canada) and Cdc42 (B-8, Santa Cruz Biotechnology), as described previously (Fera et al., 2004). To test for association with Nampt, GTP-bound Cdc42/Rac1 was affinity precipitated from 3 mg of total protein lysate and precipitated proteins, as well as whole-cell lysates were separated on 4–20% SDS-PAGE, transferred to PVDF membrane, and immunoblotted using primary antibody against Nampt or Cdc42. Protein A/G PLUS agarose (Santa Cruz) was used as negative control. Knockdown of Cdc42 was undertaken using siRNA against Cdc42 or control siRNA (Silencer® Select Validated siRNA and Negative Control No. 1 siRNA, 50 nM, Applied Biosystems, Burlington, Canada) delivered by electroporation (Amaxa Nucleofector, Lonza, Allendale, NJ).

In situ assessment of Nampt–Cdc42 colocalization

Nampt–Cdc42 colocalization was assessed *in situ* by proximity ligation assay (Duolink, Olink Bioscience, Uppsala, Sweden). Briefly, SMCs were fixed with 4% paraformaldehyde and permeablized with 0.5% Triton X-100. After blocking with 5% normal goat serum, cells were incubated with primary antibodies against

Nampt (1:400; Bethyl Laboratories) and Cdc42 (1:80, B-8; Santa Cruz, Santa Cruz, CA) for 1 h. Thereafter, cells were incubated with proximity ligation assay (PLA) anti-rabbit PLUS and anti-mouse MINUS probes, followed by ligation and amplification reactions according to the manufacturer's specifications, using the red (598/634 nm) *in situ* detection agent. Cells were subsequently incubated with FITC-conjugated phalloidin to visualize actin microfilament bundles. The extent to which Cdc42 and Nampt were colocalized was quantified using ImageJ, as the total fluorescence intensity per cell, averaged from at least 150 cells. Background signal was determined from cells subjected to the ligation assay using only the anti-Nampt primary antibody or only the anti-Cdc42 antibody.

Statistical analysis

Data are expressed as means ± s.e.m. Significant differences were assessed by Student's *t*-test or analysis of variance with a Bonferonni *post hoc* test.

Funding

This work was supported by the Heart and Stroke Foundation of Canada [grant number T7081 to J.G.P. and Research Fellowship to H.Y.]; the Canadian Institutes of Health Research [grant number FRN-11715 to J.G.P.]; Western University Department of Medicine Program of Experimental Medicine (POEM) Research Award (to J.G.P.); and the Heart and Stroke Foundation of Ontario - Barnett/Ivey Chair (to J.G.P.).

Supplementary material available online at
http://jcs.biologists.org/lookup/suppl/doi:10.1242/jcs.110262/-/DC1

References

Berger, F., Lau, C., Dahlmann, M. and Ziegler, M. (2005). Subcellular compartmentation and differential catalytic properties of the three human nicotinamide mononucleotide adenylyltransferase isoforms. *J. Biol. Chem.* **280**, 36334-36341.

Bogan, K. L. and Brenner, C. (2008). Nicotinic acid, nicotinamide, and nicotinamide riboside: a molecular evaluation of NAD+ precursor vitamins in human nutrition. *Annu. Rev. Nutr.* **28**, 115-130.

Borradaile, N. M. and Pickering, J. G. (2009). NAD(+), sirtuins, and cardiovascular disease. *Curr. Pharm. Des.* **15**, 110-117.

Cantarella, C., Sepe, L., Fioretti, F., Ferrari, M. C. and Paolella, G. (2009). Analysis and modelling of motility of cell populations with MotoCell. *BMC Bioinformatics* **10**, S12.

Costford, S. R., Bajpeyi, S., Pasarica, M., Albarado, D. C., Thomas, S. C., Xie, H., Church, T. S., Jubrias, S. A., Conley, K. E. and Smith, S. R. (2010). Skeletal muscle NAMPT is induced by exercise in humans. *Am. J. Physiol. Endocrinol. Metab.* **298**, E117-E126.

Dickson, B. C. and Gotlieb, A. I. (2003). Towards understanding acute destabilization of vulnerable atherosclerotic plaques. *Cardiovasc. Pathol.* **12**, 237-248.

Espinosa-Tanguma, R., O'Neil, C., Chrones, T., Pickering, J. G. and Sims, S. M. (2011). Essential role for calcium waves in migration of human vascular smooth muscle cells. *Am. J. Physiol. Heart Circ. Physiol.* **301**, H315-H323.

Etienne-Manneville, S. and Hall, A. (2001). Integrin-mediated activation of Cdc42 controls cell polarity in migrating astrocytes through PKCzeta. *Cell* **106**, 489-498.

Falk, E., Shah, P. K. and Fuster, V. (1995). Coronary plaque disruption. *Circulation* **92**, 657-671.

Fera, E., O'Neil, C., Lee, W., Li, S. and Pickering, J. G. (2004). Fibroblast growth factor-2 and remodeled type I collagen control membrane protrusion in human vascular smooth muscle cells: biphasic activation of Rac1. *J. Biol. Chem.* **279**, 35573-35582.

Ferns, G. A. A., Raines, E. W., Sprugel, K. H., Motani, A. S., Reidy, M. A. and Ross, R. (1991). Inhibition of neointimal smooth muscle accumulation after angioplasty by an antibody to PDGF. *Science* **253**, 1129-1132.

Goody, M. F., Kelly, M. W., Lessard, K. N., Khalil, A. and Henry, C. A. (2010). Nrk2b-mediated NAD+ production regulates cell adhesion and is required for muscle morphogenesis in vivo: Nrk2b and NAD+ in muscle morphogenesis. *Dev. Biol.* **344**, 809-826.

Heberlein, K. R., Han, J., Straub, A. C., Best, A. K., Kaun, C., Wojta, J. and Isakson, B. E. (2012). A novel mRNA binding protein complex promotes localized plasminogen activator inhibitor-1 accumulation at the myoendothelial junction. *Arterioscler. Thromb. Vasc. Biol.* **32**, 1271-1279.

Imai, S. and Guarente, L. (2010). Ten years of NAD-dependent SIR2 family deacetylases: implications for metabolic diseases. *Trends Pharmacol. Sci.* **31**, 212-220.

Khan, J. A., Tao, X. and Tong, L. (2006). Molecular basis for the inhibition of human NMPRTase, a novel target for anticancer agents. *Nat. Struct. Mol. Biol.* **13**, 582-588.

Kitani, T., Okuno, S. and Fujisawa, H. (2003). Growth phase-dependent changes in the subcellular localization of pre-B-cell colony-enhancing factor. *FEBS Lett.* **544**, 74-78.

Koch-Nolte, F., Fischer, S., Haag, F. and Ziegler, M. (2011). Compartmentation of NAD+-dependent signalling. *FEBS Lett.* **585**, 1651-1656.

Lee, H. C. (2004). Multiplicity of Ca2+ messengers and Ca2+ stores: a perspective from cyclic ADP-ribose and NAADP. *Curr. Mol. Med.* **4**, 227-237.

Leung, W. C., Lawrie, A., Demaries, S., Massaeli, H., Burry, A., Yablonsky, S., Sarjeant, J. M., Fera, E., Rassart, E., Pickering, J. G. et al. (2004). Apolipoprotein D and platelet-derived growth factor-BB synergism mediates vascular smooth muscle cell migration. *Circ. Res.* **95**, 179-186.

Li, S., Sims, S., Jiao, Y., Chow, L. H. and Pickering, J. G. (1999). Evidence from a novel human cell clone that adult vascular smooth muscle cells can convert reversibly between noncontractile and contractile phenotypes. *Circ. Res.* **85**, 338-348.

Li, S., Chow, L. H. and Pickering, J. G. (2000). Cell surface-bound collagenase-1 and focal substrate degradation stimulate the rear release of motile vascular smooth muscle cells. *J. Biol. Chem.* **275**, 35384-35392.

Li, S., Fan, Y. S., Chow, L. H., Van Den Diepstraten, C., van Der Veer, E., Sims, S. M. and Pickering, J. G. (2001). Innate diversity of adult human arterial smooth muscle cells: cloning of distinct subtypes from the internal thoracic artery. *Circ. Res.* **89**, 517-525.

Moissoglu, K. and Schwartz, M. A. (2006). Integrin signalling in directed cell migration. *Biol. Cell* **98**, 547-555.

Naghavi, M., Libby, P., Falk, E., Casscells, S. W., Litovsky, S., Rumberger, J., Badimon, J. J., Stefanadis, C., Moreno, P., Pasterkamp, G. et al. (2003). From vulnerable plaque to vulnerable patient: a call for new definitions and risk assessment strategies: Part I. *Circulation* **108**, 1664-1672.

Nikiforov, A., Dölle, C., Niere, M. and Ziegler, M. (2011). Pathways and subcellular compartmentation of NAD biosynthesis in human cells: from entry of extracellular precursors to mitochondrial NAD generation. *J. Biol. Chem.* **286**, 21767-21778.

Nishimura, T., Yamaguchi, T., Kato, K., Yoshizawa, M., Nabeshima, Y., Ohno, S., Hoshino, M. and Kaibuchi, K. (2005). PAR-6-PAR-3 mediates Cdc42-induced Rac activation through the Rac GEFs STEF/Tiam1. *Nat. Cell Biol.* **7**, 270-277.

Pankov, R., Endo, Y., Even-Ram, S., Araki, M., Clark, K., Cukierman, E., Matsumoto, K. and Yamada, K. M. (2005). A Rac switch regulates random versus directionally persistent cell migration. *J. Cell Biol.* **170**, 793-802.

Peters, M. W., Canham, P. B. and Finlay, H. M. (1983). Circumferential alignment of muscle cells in the tunica media of the human brain artery. *Blood Vessels* **20**, 221-233.

Petrie, R. J., Doyle, A. D. and Yamada, K. M. (2009). Random versus directionally persistent cell migration. *Nat. Rev. Mol. Cell Biol.* **10**, 538-549.

Pickering, J. G., Uniyal, S., Ford, C. M., Chau, T., Laurin, M. A., Chow, L. H., Ellis, C. G., Fish, J. and Chan, B. M. (1997). Fibroblast growth factor-2 potentiates vascular smooth muscle cell migration to platelet-derived growth factor: upregulation of alpha2beta1 integrin and disassembly of actin filaments. *Circ. Res.* **80**, 627-637.

Prager-Khoutorsky, M., Lichtenstein, A., Krishnan, R., Rajendran, K., Mayo, A., Kam, Z., Geiger, B. and Bershadsky, A. D. (2011). Fibroblast polarization is a matrix-rigidity-dependent process controlled by focal adhesion mechanosensing. *Nat. Cell Biol.* **13**, 1457-1465.

Revollo, J. R., Grimm, A. A. and Imai, S. (2004). The NAD biosynthesis pathway mediated by nicotinamide phosphoribosyltransferase regulates Sir2 activity in mammalian cells. *J. Biol. Chem.* **279**, 50754-50763.

Rocnik, E. F., Chan, B. M. and Pickering, J. G. (1998). Evidence for a role of collagen synthesis in arterial smooth muscle cell migration. *J. Clin. Invest.* **101**, 1889-1898.

Rocnik, E. F., van der Veer, E., Cao, H., Hegele, R. A. and Pickering, J. G. (2002). Functional linkage between the endoplasmic reticulum protein Hsp47 and procollagen expression in human vascular smooth muscle cells. *J. Biol. Chem.* **277**, 38571-38578.

Rongvaux, A., Galli, M., Denanglaire, S., Van Gool, F., Drèze, P. L., Szpirer, C., Bureau, F., Andris, F. and Leo, O. (2008). Nicotinamide phosphoribosyl transferase/pre-B cell colony-enhancing factor/visfatin is required for lymphocyte development and cellular resistance to genotoxic stress. *J. Immunol.* **181**, 4685-4695.

Smith, S. (2001). The world according to PARP. *Trends Biochem. Sci.* **26**, 174-179.

Söderberg, O., Gullberg, M., Jarvius, M., Ridderstråle, K., Leuchowius, K. J., Jarvius, J., Wester, K., Hydbring, P., Bahram, F., Larsson, L. G. et al. (2006). Direct observation of individual endogenous protein complexes in situ by proximity ligation. *Nat. Methods* **3**, 995-1000.

Thakar, R. G., Cheng, Q., Patel, S., Chu, J., Nasir, M., Liepmann, D., Komvopoulos, K. and Li, S. (2009). Cell-shape regulation of smooth muscle cell proliferation. *Biophys. J.* **96**, 3423-3432.

van der Veer, E., Nong, Z., O'Neil, C., Urquhart, B., Freeman, D. and Pickering, J. G. (2005). Pre-B-cell colony-enhancing factor regulates NAD+-dependent protein deacetylase activity and promotes vascular smooth muscle cell maturation. *Circ. Res.* **97**, 25-34.

van der Veer, E., Ho, C., O'Neil, C., Barbosa, N., Scott, R., Cregan, S. P. and Pickering, J. G. (2007). Extension of human cell lifespan by nicotinamide phosphoribosyltransferase. *J. Biol. Chem.* **282**, 10841-10845.

Wei, C., Wang, X., Chen, M., Ouyang, K., Song, L. S. and Cheng, H. (2009). Calcium flickers steer cell migration. *Nature* **457**, 901-905.

Yang, H., Yang, T., Baur, J. A., Perez, E., Matsui, T., Carmona, J. J., Lamming, D. W., Souza-Pinto, N. C., Bohr, V. A., Rosenzweig, A. et al. (2007). Nutrient-sensitive mitochondrial NAD+ levels dictate cell survival. *Cell* **130**, 1095-1107.

Ziegler, M. (2000). New functions of a long-known molecule. Emerging roles of NAD in cellular signaling. *Eur. J. Biochem.* **267**, 1550-1564.